Particle Accelerators, 1987, Vol. 21, pp. 197–226
Photocopying permitted by license only

Printed in the United States of America

INTERNAL DYNAMICS AND EMITTANCE GROWTH IN SPACE-CHARGE-DOMINATED BEAMS

O. A. ANDERSON
Lawrence Berkeley Laboratory, University of California, Berkeley, CA 94720

(Received January 31, 1986; in final form September 25, 1986)

Previous analytical studies have related transverse rms emittance growth in nonuniform beams to changes in the beam density profile, but the time evolution of the process has not been analyzed. Our new approach analyzes the internal motion of the beam and from this obtains the explicit time dependence of the rms emittance. It is shown to reach its peak value explosively in about one quarter of a plasma period. The subsequent behavior depends on the uniformity of the initial density profile. We derive a uniformity criterion that determines whether or not the emittance oscillates periodically and present examples of density profiles for which the emittance returns to its initial value and then continues to oscillate. We discuss a class of continuous initial profiles that lead to discontinuous shocklike behavior (with partial irreversibility of the oscillations) and a class of segmented profiles for which the emittance jumps to its maximum value in one fourth of a plasma period and remains at that value with essentially no further change.

1. INTRODUCTION

Analytical studies of rms emittance arising out of space-charge field energy began with the pioneering work of Lapostolle.[1] His treatment utilized the rms envelope equations developed by him and by Sacherer.[2] Since then, Lee[3] and, more recently, Wangler *et al.*[4] have done independent analyses. These authors found a differential equation relating changes in emittance to changes in the self-field energy. Wangler *et al.* also presented numerical simulations showing emittance growth in one quarter of a plasma period. This surprisingly rapid growth was unexplained by the analysis.

In the previous reports, moments were calculated and relationships were deduced among their time derivatives. Since these equations were not closed, time-dependent solutions could not be obtained. With the present method, we first solve for the beam internal motion as a function of time and then calculate the moments. The rms emittance found from these moments is shown to reach its peak value in about one quarter of a plasma period, in agreement with the simulations of Wangler *et al.*

We separate the mean square emittance into a thermal part and a fluid part. For a strongly space-charge-dominated warm beam, the fluid motion during emittance growth is the same as for the corresponding cold beam, except for a slight change in timing. Thus, we do almost all of the analysis on cold beams, gaining mathematical simplicity. After calculating the explicit time dependence of the cold-beam emittance, we add in the thermal part and obtain a complete treatment of the explosive stage of emittance growth in bright beams.

To simplify the formulas in the present treatment, the beam is assumed to be nonrelativistic. (However, this restriction is easily removed by applying the relativistic correction factor γ^{-3} to the final result for mean square emittance.) The beam energy is assumed to be much larger than the space-charge potential, allowing the usual approximation that all beam particles have the same energy and the same constant longitudinal velocity v. This assumption also implies that all transverse velocities are much smaller than v.

We treat steady flow; i.e., at a given point z in the longitudinal direction, there are no changes with time. Changes occur when following the beam at velocity v, so that "time" in this paper simply means z/v.

Our beam propagates in vacuum; a modification would be needed if the beam were partially neutralized by background plasma. For vacuum propagation, the self-magnetic field force is v^2/c^2 times the self-electrostatic force and is therefore neglected; the correction factor to the self-force would be γ^{-2}. Combining this with the relativistic mass correction would give the factor γ^{-3} mentioned above.

We treat both round beams and sheet beams. Round beams by definition are azimuthally symmetric, and sheet beams by assumption are symmetric in the direction of transverse motion, x. This symmetry means that only the upper half ($x \geq 0$) of a sheet beam needs to be considered; all x-integrals start from zero.

We start with sheet-beam dynamics (Section 2) because the equations are simpler and exact results are obtained. These exact results give a good background for the perturbation analysis of round-beam dynamics in Section 3.

2. SHEET BEAMS

2.1. Space-Charge Field

If the beam density is $n(x, z)$, the number of particles per square centimeter within half-width x is

$$N_x(x, z) = \int_0^x n(x_1, z)\, dx_1, \tag{1}$$

and the total number per square centimeter is

$$N = \int_0^\infty n(x, z)\, dx, \tag{2}$$

which is constant for steady flow. Equation (1) means that

$$n = \partial N_x / \partial x.$$

If all beam particles have the same charge e, Poisson's equation is

$$\partial N_x / \partial x = (4\pi e)^{-1} (\partial / \partial x) E_S(x, z),$$

where E_S is the x-component of the space-charge field. The term $\partial E_{Sz}/\partial z$ has been dropped. This is justifiable if the beam is reasonably thin, i.e., if $(kh)^2 \ll 1$,

where k is the channel-focusing wave number and h is the beam half-width. Integrating, we have

$$E_S = 4\pi e N_x. \tag{3}$$

A basic quantity is the normalized line perveance

$$P = 4\pi N e^2/mv^2. \tag{4}$$

2.2. *Particle Motion*

As stated in the introduction, we begin by analyzing cold beams; thermal motion will be included later. We consider particles in a uniform channel experiencing a self-consistent space-charge force and a linear external focusing force F_e. We define the focusing constant k^2 by

$$F_e/mv^2 = -k^2 x, \tag{5}$$

so that

$$x'' \equiv d^2x/dz^2 = -k^2 x + eE_S/mv^2 \tag{6}$$

or, from Eqs. (3) and (4),

$$x'' + k^2\left[x - \frac{P}{k^2}\frac{N_x(x, z)}{N}\right] = 0. \tag{7}$$

For a cold beam, the particle motion is initially laminar. We show in Section 2.3 that it remains laminar for at least a distance $\lambda/4$, where $\lambda = 2\pi/k$; λ is also shown to be the distance the beam travels in one period of plasma oscillation. We will find that the peak rms emittance occurs at $\lambda/4$, while the motion is still laminar.

Thus, we begin with the assumption of laminar motion over a range $0 \le z \le z_c$, where the critical distance $z_c > \lambda/4$ is to be calculated later. Since no trajectories cross, N_x is preserved for each particle at its position $x(z)$.

If we write ξ for the initial position of the particle that is currently at $x(z)$, then $N_x(x, z) = N_x(\xi, 0)$ for all x in the laminar range of z, so that the last term in Eq. (7) (the space-charge term) is constant. Using the abbreviation $N_x(x, 0) = N_x(\xi)$, we define the equilibrium position

$$x_e(\xi) = \frac{P}{k^2}\frac{N_x(\xi)}{N} \tag{8}$$

and get the linear equation

$$x'' + k^2[x - x_e(\xi)] = 0 \tag{9}$$

for the range $[0, z_c]$. The solution, for the initial condition $x'(\xi) = 0$, is

$$x(\xi, z) = x_e(\xi) + [\xi - x_e(\xi)] \cos kz. \tag{10}$$

From Eqs. (8) and (10), at $z = \lambda/4$ the position of the beam edge is

$$x(h, \lambda/4) = x_e(h) = P/k^2, \tag{11}$$

so that P/k^2 is the beam width at $z = \lambda/4$. That is, P/k^2 is the center of oscillation of the beam edge during the period of laminar motion. P/k^2 is a basic unit of length, which has several other interpretations mentioned further on.

Differentiating Eq. (10) with respect to z yields

$$x'(\xi, z) = -k[\xi - x_e(\xi)] \sin kz, \tag{12}$$

which will be used below. But first, we investigate the duration of laminarity.

2.3. *Trajectory Crossing for Continuous Profile*

Laminar particle motion ceases when two beam elements with an initial separation $d\xi$ are later separated by $dx = 0$, i.e., when the derivative $dx/d\xi$ vanishes. From Eq. (10),

$$dx/d\xi = dx_e/d\xi + (1 - dx_e/d\xi) \cos kz. \tag{13}$$

From Eqs. (1) and (8),

$$\frac{dx_e}{d\xi} = \frac{n(\xi)}{n_u}, \tag{14}$$

where

$$n_u = \frac{N}{P/k^2}. \tag{15}$$

It turns out that n_u is the density of a cold, uniform, matched beam, giving another interpretation for P/k^2. Also, we will find that n_u is the density of the actual cold beam at $z = \lambda/4$.

We use n_u to define the plasma frequency ω_{p0}:

$$\omega_{p0}^2 = 4\pi e^2 n_u/m.$$

The distance that the beam travels in one plasma period is $\lambda_{p0} = 2\pi v/\omega_{p0}$. Using Eqs. (4) and (15), we see that $\lambda_{p0} = 2\pi/k$, which is the same as λ, defined earlier.

Combining Eqs. (13) and (14),

$$dx/d\xi = n(\xi)/n_u + [1 - n(\xi)/n_u] \cos kz. \tag{16}$$

Laminar motion ceases at the critical distance z_c where $dx/d\xi$ first vanishes:

$$\cos kz_c = \frac{-1}{n_u/n(\xi_c) - 1}. \tag{17}$$

In Eq. (17), ξ_c is the point of minimum initial n; particles originating in the neighborhood of ξ_c are the first to cross trajectories if such crossing occurs.

Laminarity criterion. If $n(\xi) > n_u/2$ for all $\xi < h$, there is no solution to Eq. (17), z_c does not exist, and the motion is laminar for all z in the cold-beam limit. If $n(\xi) \leq n_u/2$ over some range of ξ, then that part of the beam with the lowest initial density, which was $n(\xi_c)$, will cross trajectories first and define z_c.

Observe that if z_c exists then its value always lies between $\lambda/4$ and $\lambda/2$. It approaches $\lambda/2$ for profiles with minimum density $n(\xi_c)$ slightly less than $n_u/2$, and approaches $\lambda/4$ for profiles with $n(\xi_c) \ll n_u/2$.

If the initial density profile gradually falls to zero at the beam edge, then $n(\xi_c) = 0$ and $z_c \to \lambda/4$. But if there is a sharp cutoff, as is typical for a cold beam, then the density at cutoff is relevant.

2.4. Beam Density Time Dependence

Laminar particle motion implies $n(x, z)\, dx = n(\xi)\, d\xi$, i.e.,

$$n(\xi)/n(x, z) = dx/d\xi. \tag{18}$$

We combine this with Eq. (16) to find the beam density z-dependence (with our constant-v model and with $z = vt$, we often use the term *time* dependence):

$$n(x, z) = \frac{n_u}{1 + [n_u/n(\xi) - 1] \cos kz}, \tag{19}$$

where the x dependence is found by simultaneous use of Eq. (10). The above result can be obtained from the fluid equations for a cold fluid. Note that $n(x)$ becomes uniform at $z = \lambda/4$, and then a density reversal occurs: Particles originating in underdense regions find themselves in overdense regions and vice versa. If the laminarity criterion is violated, then $n \to \infty$ as $z \to z_c$ for particles originating at ξ_c. Equation (7) is no longer linear for $z > z_c$, and Eq. (19) becomes inapplicable. After z_c a shocklike phenomenon occurs, which is illustrated further on.

2.5. Segmented Density Profile

In practical applications, it may be necessary to merge several beams into one channel. In such cases, the initial beam profile $n(\xi)$ may have gaps where the density vanishes, and the above treatment must be slightly modified. Instead of considering two beam elements initially separated by an infinitesimal distance $d\xi$, we need to consider elements separated by a finite distance $\Delta\xi$. In Eq. (13), we replace $dx_e/d\xi$ by $\Delta x_e/\Delta\xi$, while Eq. (14) becomes

$$\frac{\Delta x_e}{\Delta\xi} = \frac{1}{\Delta\xi} \int_{\xi}^{\xi+\Delta\xi} \frac{n(\xi_1)\, d\xi_1}{n_u} = \frac{\langle n(\xi) \rangle}{n_u}, \tag{20}$$

with the average taken over the range $\Delta\xi$. We find

$$\frac{\Delta x}{\Delta\xi} = \frac{\langle n(\xi) \rangle}{n_u} + \left[1 - \frac{\langle n(\xi) \rangle}{n_u}\right] \cos kz, \tag{21}$$

which agrees with Eq. (16) if the profile is continuous and if $\Delta\xi \to 0$. If $\Delta\xi$ extends exactly from one edge of a gap to the other, then it contains no particles and $\langle n(\xi)\rangle = 0$. Equation (21) shows that Δx will be zero at the critical distance $z_c = \lambda/4$.

Summarizing: For a segmented profile, the gaps close at $\lambda/4$. The density is uniform there just as in the case of continuous profiles. Unlike that case, the density does not become infinite when the trajectories start to cross.

In the remainder of this paper, we assume unless stated otherwise that the profile is continuous. The above discussion indicates the sort of modification, if any, that is needed to treat beams with gaps.

2.6. Density and Transverse Velocity at $\lambda/4$

Interesting phenomena occur at $z = \lambda/4$. At that point, the beam has uniform density and maximum transverse velocities. Eq. (19) shows that

$$n(x, \lambda/4) = n_u. \tag{22}$$

Thus, for any cold-beam initial profile, continuous or not, matched or not, the density at $\lambda/4$ is uniform and equal to the density of a matched beam. This surprising result comes from the linearity of Eq. (9) and is not quite true for round beams. We shall see later that this result is important because it means that the free electrostatic energy has its minimum value at $\lambda/4$ (and therefore the kinetic energy is maximum).

It is obvious from Eq. (12) that any particle has its peak transverse velocity at $\lambda/4$. We can also show, by differentiating Eq. (12) with respect to ξ, that the particular particle with the largest velocity originates at the point ξ_m where the initial density $n(\xi_m) = n_u$. (There may be several such points.)

The largest peak velocity, written in dimensionless form, is

$$x'_{\max} = -k[\xi_m - N_x(\xi_m)/n_u]. \tag{23}$$

2.7. Rms Beam Size

Averages over density profiles are defined by

$$\langle g\rangle(z) = N^{-1}\int_0^\infty dx\, n(x, z)g(x). \tag{24}$$

Changing the integration variable from x to the initial value ξ gives

$$\langle g\rangle(z) = N^{-1}\int_0^\infty d\xi\, n(\xi)g(x(\xi, z)). \tag{25}$$

For the mean square beam width, we use the notation

$$X^2(z) = \langle x^2\rangle = N^{-1}\int_0^\infty d\xi\, n(\xi)x^2(\xi, z). \tag{26}$$

If we abbreviate Eq. (10) as

$$x(\xi, z) = x_e(1 - C) + \xi C, \tag{27}$$

where $C = \cos kz$, then

$$\begin{aligned} X^2 &= N^{-1} \int_0^\infty d\xi\, n(\xi)[x_e^2(1 - C)^2 + 2\xi x_e C(1 - C) + \xi^2 C^2] \\ &= (P^2/3k^4)(1 - C)^2 + (2W_0/k^2)C(1 - C) + X_0^2 C^2. \end{aligned} \tag{28}$$

The first term on the right is obtained by using Eq. (14) and integrating by parts. The second term is proportional to the virial moment[3] derived for sheet beams in Appendix A:

$$W(z) = \langle K_S x^2 \rangle = (P/2N^2) \int_0^\infty dx(N^2 - N_x^2). \tag{29}$$

Note that W_0 means $W(0)$. The third term involves X_0, the initial value of the rms beam size X.

We can rewrite Eq. (28) in terms of the normalized free self-field energy (beam shape factor) defined in Appendix A, Eq. (A-24):

$$U_n(z) = 2(1 - \sqrt{3}W/PX). \tag{30}$$

Writing $U_n(0) = U_{n0}$, we get

$$X^2(z) = \left[\frac{P}{\sqrt{3}k^2}(1 - C) + X_0 C\right]^2 - U_{n0} X_0 \frac{P}{\sqrt{3}k^2} C(1 - C). \tag{31}$$

The rms beam size given by Eq. (31) is exact during the period of laminar motion defined by Eq. (17), which extends at least to $z = \lambda/4$; if the corresponding criterion $n(\xi) > n_u/2$ is satisfied for all ξ, then Eq. (31) applies for all z.

Equation (31) is greatly simplified for a matched beam.

2.8. *Matching*

In Eq. (31), whatever value of X_0 is chosen, there will be fluctuations in X (unless the initial profile is uniform). But certain choices give a matched beam in the sense that the fluctuations are quite small. Two choices, which are particularly simple, are discussed here. The first, which gives what we call $\lambda/4$ matching, is the same as matching based on the equivalent-beam concept[1,2,4] while the second, which we call $\lambda/2$ matching, gives less than half as much ripple. Either choice simplifies the form of Eq. (28) or (31).

2.8.1. $\lambda/4$ matching. For this case, we choose X_0, the value of X at $z = 0$, to be equal to the value given by Eq. (31) at $z = \lambda/4$:

$$X_0^2 = X^2(\lambda/4) = \frac{1}{3}\left(\frac{P}{k^2}\right)^2. \tag{32}$$

Using this result in Eq. (31) gives

$$X^2(z) = X_0^2[1 - U_{n0}\cos kz(1 - \cos kz)]. \tag{33}$$

If we define the ripple factor

$$F_r = \frac{X_{\max}^2 - X_{\min}^2}{X_0^2}, \tag{34}$$

then we find for $\lambda/4$ matching

$$F_r = (9/4)U_{n0}. \tag{35}$$

2.8.2. $\lambda/2$ matching. We choose the initial value of X to equal the value given by Eq. (31) at $z = \lambda/2$. Solving the resulting equation for X_0 gives

$$X_0 = (P/\sqrt{3}k^2)(1 - U_{n0}/2)^{-1}. \tag{36}$$

Inserting this in Eq. (31) yields

$$X^2(z) = X_0^2[1 - U_{n0}(1 - U_{n0}^2/4)\sin^2 kz]. \tag{37}$$

In this case, we obviously have the ripple factor

$$F_r = U_{n0}(1 - U_{n0}^2/4). \tag{38}$$

This can be shown to be the smallest possible value. It is less than half the value given by Eq. (35) for $\lambda/4$ matching or equivalent-beam matching.

Of course, Eqs. (36) and (37) are exact up to $\lambda/2$ only if the laminarity criterion under Eq. (17) is satisfied. But they may be useful even in cases where laminar motion breaks down.

2.9. Rms Emittance

We use Sacherer's definition of mean square emittance[2]:

$$\epsilon^2 = \langle x^2\rangle\langle x'^2\rangle - \langle xx'\rangle^2. \tag{39}$$

The method that we used to find $\langle x^2\rangle$ [Eq. (28)] gives for the other moments

$$\langle x'^2\rangle = (P^2/3k^4 - 2W_0/k^2 + X_0^2)k^2\sin^2 kz,$$
$$\langle xx'\rangle = [(P^2/3k^4)(1 - C) + (W_0/k^2)(2C - 1) - X_0^2C]k\sin kz,$$

assuming $z < z_C$. Many terms cancel when these two equations and Eq. (28) are inserted in Eq. (39). We are left with

$$\epsilon^2(z) = \frac{P^2}{k^2}\left[\frac{X_0^2}{3} - \frac{W_0^2}{P^2}\right]\sin^2 kz. \tag{40}$$

This form is useful for some calculations. But with the aid of Eq. (30) a more interesting version is obtained, which shows the connection between the rms

emittance and the free self-field energy U_{n0}:

$$\epsilon^2(z) = \frac{P^2 X_0^2}{3k^2} U_{n0}\left(1 - \frac{U_{n0}}{4}\right) \sin^2 kz. \tag{41}$$

Equations (40) and (41) apply whether the beam is matched or not. If we specify as a special case that the beam is $\lambda/4$ matched, then Eq. (32) gives for $z < z_C$

$$\epsilon^2(z) = \frac{P}{\sqrt{3}} X_0^3 U_{n0}\left(1 - \frac{U_{n0}}{4}\right) \sin^2 kz, \tag{42}$$

which has a close relationship to the differential equation for emittance [Eq. (A-25)] derived in Appendix A:

$$\frac{d}{dz}\epsilon^2 = -\frac{P}{\sqrt{3}} X^3(z) \frac{d}{dz} U_n.$$

The factor $(1 - U_{n0}/4)$ for typical initial beam profiles is usually within about 1% of unity. This factor arises from the small variations of X given by Eq. (33).

To find $\epsilon(z)$, we take the positive square root of Eq. (42), so that $\epsilon(z) \propto |\sin kz|$. If the laminarity criterion is satisfied, this time dependence continues indefinitely.

2.10. Irreversible Behavior (Wave Breaking)

In this section, we discuss cases where $n(\xi)$ is nonvanishing out to the beam edge but where $n(\xi) < n_u/2$ for some ξ; Eq. (17) gives the point $z = z_C$ where the trajectories will cross. As we have shown, the phase-space dynamics of cold beams are easily and exactly described up to this point. Before z_C is reached, the distribution on the (x, x') phase plane is a well-behaved curve with slope

$$\frac{dx'}{dx} = \frac{dx'/d\xi}{dx/d\xi} = \frac{-[1 - n(\xi)/n_u]k \sin kz}{n(\xi)/n_u + [1 - n(\xi)/n_u] \cos(kz)}. \tag{43}$$

Comparison with Eq. (17) shows that this slope is finite for $z < z_C$, so that $x'(x)$ is single-valued. As $z \to z_C$ the curve steepens like the shape of a wave about to break. Although this occurs in phase space, not real space, the subsequent behavior is sometimes referred to as wave breaking.[5] In real space, the cold-beam equation [Eq. (19)] shows that the charge density becomes singular as $z \to z_C$.

Although our main purpose here is to present analytic results, we show a typical numerical simulation[6] to illustrate the effect. Figure 1a shows the steepening of dx'/dx and the wave breaking in phase space. Immediately after z_C, $x'(x)$ becomes triple-valued near $x = 0$; this implies the sudden appearance there of a finite pressure tensor (see Section 2.14). Indeed, the density profiles in Fig. 1b exhibit phenomena resembling shock fronts propagating from the singularity.

Returning to the analysis, it should be noted that, for $z > z_C$, Eq. (7) must be used; the linear equation [Eq. (9)] and all its consequences are inapplicable.

When the laminarity criterion is satisfied, there is no wave breaking and Eq.

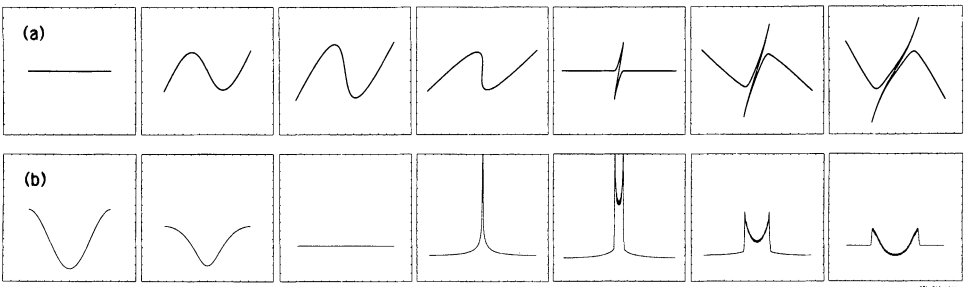

FIGURE 1 Example of (a) wave breaking in phase space and (b) shock formation in configuration space. Upper row shows phase plots (i.e., x' vs x) at $z/\lambda = 0.0$, 0.125, 0.25, 0.375, 0.5, 0.625, and 0.75; lower row shows corresponding charge densities. The initial density profile was chosen to be $n/n_u = 1 - 0.7\cos(\pi\xi/h)$ for $\xi \leq h$, with $n = 0$ for $\xi > h$. The results during the laminar regime agree with Eqs. (43) and (19). According to Eq. (17), wave breaking starts at $z_C = 0.32\lambda$ for this initial profile. This figure illustrates cold-beam behavior. Space-charge-dominated warm-beam results are similar to these except that the shock like structures are smoother.

(42) continues to apply. There is reversible exchange between electrostatic energy and laminar motion, and the emittance periodically returns to zero. But when wave breaking occurs, one may expect some irreversibility or damping of these oscillations, and this has been observed using numerical simulation.[6]

The above remarks apply to continuous density distributions. In the case of segmented beams, there is extremely strong damping of the emittance oscillations (i.e., nearly complete irreversibility), as discussed in the next section. This situation occurs when beams from several sources are merged in the same channel.

2.11. Multiple Sheet Beams in One channel

It has been proposed recently for some applications to merge separate beamlets into a single transport or acceleration channel. For example, one proposal, from Oak Ridge National Laboratory, involves sheet beams, while others, from Lawrence Berkeley Laboratory and from JAERI, involve round beams. Our discussion in this section indicates what can happen in either case: prompt, permanent, and substantial emittance growth. In a later section, we evaluate this growth using typical parameters for these applications.

We can use the above analysis to draw some general conclusions. If a number of uniform, separated beamlets are introduced into a channel, Eq. (21) shows that the gaps close at $\lambda/4$, so that the overall density becomes uniform at that moment. In the phase plane, each beamlet remains a straight line but is tilted with slope

$$\frac{dx'}{dx} = \frac{-k[1 - n(\xi)/n_u]}{n(\xi)/n_u}. \tag{44}$$

Immediately after $z = \lambda/4$, the beamlets start to overlap. The acquired momentum causes this overlapping to increase with time; obviously the original gaps

never appear again. One may expect then that after $\lambda/4$ the density profile remains approximately constant, i.e., the emittance remains near the maximum value that occurred at $\lambda/4$.

Figure 2a, obtained by numerical simulation,[6] illustrates these points. It shows ϵ vs z/λ for six uniform beams injected into one channel. Up to $\lambda/4$, the simulation agrees with Eq. (42) or, in particular, with Eq. (48), derived below.

In contrast, Fig. 2b shows the result for a single beam with profile $n/n_u = 1.2 - 0.6\xi^2$ for $\xi < 1$, satisfying the laminarity criterion. There is complete reversibility and the simulation agrees exactly with Eq. (42).

To analyze the emittance for a segmented beam, we choose the simplest model: M segments, each with the same uniform density and the same width, and separated by distances equal to this width. We find for this case

$$U_{n0} = 2 - \frac{2}{M}\frac{2M^2 - 1}{(4M^2 - 3)^{1/2}}. \tag{45}$$

When the number M becomes large, $U_{n0} \cong 1/(4M^2)$. The rms emittance is

$$\epsilon(z) = \frac{hP}{2k}\frac{(M^2 - 1)^{1/2}}{M(2M - 1)}\sin kz, \tag{46}$$

which of course applies only up to $z = \lambda/4$, so absolute-value bars are omitted. In Eq. (46), h stands for the initial half-width of the entire set of beamlets.

The condition for $\lambda/4$ matching is

$$h = \frac{P}{k^2}\frac{2M - 1}{(4M^2 - 3)^{1/2}}. \tag{47}$$

For such matching, Eq. (46) becomes

$$\epsilon(z) = \frac{P^2}{3k^3}\frac{1}{M}\left[\frac{M^2 - 1}{4M^2 - 3}\right]^{1/2}\sin kz \tag{48}$$

for $z \leq \lambda/4$. Expanding Eq. (49) for large M,

$$\epsilon(z) = \frac{P^2}{6k^3M}\left[1 - \frac{1}{8M^2} + \cdots\right]\sin kz \tag{49}$$

for $z \leq \lambda/4$. Thus $\epsilon \propto 1/M$ for $M > 3$.

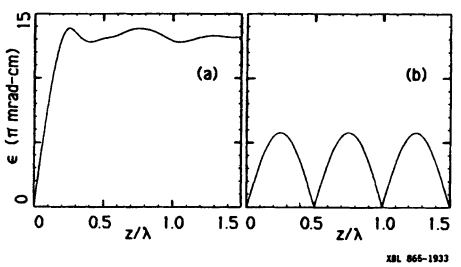

FIGURE 2 (a) Irreversible behavior of emittance for segmented beam; (b) reversible behavior for continuous profile.

It should not be surprising that $\epsilon \to 0$ for large M, since a continuous beam actually consists of a very large number of individual beamlets (particles).

2.12. *Rms Emittance of a Warm Sheet Beam*

We define the "standard" uniform-beam equilibrium distribution function to be

$$f(x, x') = \frac{n_b}{\pi x_0'}\left(1 - \frac{x^2}{x_0^2} - \frac{x'^2}{x_0'^2}\right)^{-1/2} \tag{50}$$

within the bounding ellipse; f is zero outside the ellipse. This function, derivable by Abel inversion, is the sheet-beam version of the K–V distribution. Integrating over dx' confirms that the beam is uniform:

$$\begin{aligned} n(x) &= n_b \quad (x \le x_0), \\ &= 0 \quad (x > x_0). \end{aligned}$$

The condition for equilibrium, according to the Vlasov equation, is

$$x_0'^2 = k^2 x_0^2 - P x_0. \tag{51}$$

(We do not discuss stability here.) Taking moments of f, we find

$$\begin{aligned} \langle x^2 \rangle &= x_0^2/3, \\ \langle x'^2 \rangle &= x_0'^2/3, \\ \langle xx' \rangle &= 0, \end{aligned}$$

and the rms emittance is

$$\epsilon = x_0 x_0'/3. \tag{52}$$

Therefore, we introduce a modified quantity

$$\epsilon_{3\text{rms}} = 3\epsilon, \tag{53}$$

which agrees with the enclosure emittance for our standard beam. This is exactly analogous to the quantity $\epsilon_{4\text{rms}}$ defined later [Eq. (114)] for round beams.

The condition for Vlasov equilibrium can then be written

$$0 = -k^2 x_0 + P + \epsilon_{3\text{rms}}^2 x_0^{-3}, \tag{54}$$

which agrees with the stationary envelope equation for a uniform sheet beam.[7] For a cold beam, the last term vanishes, and we have yet another meaning for P/k^2:

$$x_0 = P/k^2.$$

2.13. *Typical Numbers*

The normalized perveance P [see Eq. (4)] can be written in terms of $I_L = 2Nev$, the total beam current per centimeter:

$$P = 4.08 \times 10^6 \frac{I_L}{V^{3/2}} \frac{A^{1/2}}{Q^{1/2}}, \tag{55}$$

with I_L in amperes/cm. The beam energy is eV, and V is in volts. A is the atomic weight and Q is the charge state of the beam particles. We are still assuming that the beam is nonrelativistic, as discussed in the introduction.

Using the matching condition, Eq. (32), in Eq. (41) allows the emittance to be expressed in terms of the basic length P/k^2. [For a beam that remains laminar, P/k^2 is the beam width averaged over a plasma period; otherwise, it is the width at $z = \lambda/4$. See Eq. (11).] Then the peak value for the emittance (squared) is

$$\epsilon_{3\text{rms}}^2 = 4.08 \times 10^6 \frac{A^{1/2}}{Q^{1/2}} \frac{I_L}{V^{3/2}} \left(\frac{P}{k^2}\right)^3 U_{n0}\left(1 - \frac{U_{n0}}{4}\right)$$

for a cold beam at $\lambda/4$. For the segmented beam case, Eq. (49), the peak emittance is

$$\epsilon_{3\text{rms}} = \frac{1.01 \times 10^3}{M} \frac{A^{1/4}}{Q^{1/4}} \frac{I_L^{1/2}}{V^{3/4}} \left(\frac{P}{k^2}\right)^{3/2}$$

if $M > 3$. For example, if $I_L = 0.2$ A/cm, $V = 10^5$ volts, and $P/k^2 = 1.0$ cm, then

$$\epsilon_{3\text{rms}} = 0.080\, A^{1/4}/(Q^{1/4}M) \quad [\pi \text{ rad-cm}]$$

in the large-M limit. The normalized emittance would be

$$\epsilon_{N3\text{rms}} = 0.84\, A^{1/4}/(Q^{1/4}M) \quad [\pi \text{ mrad-cm}].$$

Clearly, segmented-beam emittances can jump to substantial values unless M, the number of beamlets, is large. For other beam profiles, $\epsilon_{3\text{rms}}$ may be calculated using U_{n0} from Eq. (30) or from Appendix A, Table A-I.

2.14. Inclusion of Thermal Emittance

In this section, we show that most of our results for cold beams are readily applied to warm beams. First, we show that, in general, the mean square emittance can be divided into a thermal part and a fluid-flow part.

For any value of x, we define the local dimensionless fluid velocity

$$u(x, z) = (x')_{\text{av}} = n(x, z)^{-1} \int_{-\infty}^{\infty} dx' x' f(x, x', z) \tag{56}$$

and the normalized specific pressure tensor

$$T(x, z) = n^{-1} \int_{-\infty}^{\infty} dx' (x' - u)^2 f(x, x', z). \tag{57}$$

For a Gaussian velocity distribution, $T(x, z)$ represents the local temperature. The local mean square velocity is

$$(x'^2)_{\text{av}} = T(x, z) + u^2(x, z).$$

Using Eq. (24) to average over x, we write

$$\langle x'^2 \rangle(z) = \langle T \rangle(z) + \langle u^2 \rangle(z).$$

For rms emittance, we also need $\langle xx' \rangle$. It is easy to show that $\langle xx' \rangle = \langle xu \rangle$, so that Eq. (39) becomes

$$\epsilon^2 = \langle x^2 \rangle \langle T \rangle + [\langle x^2 \rangle \langle u^2 \rangle - \langle xu \rangle^2]. \tag{58}$$

Note that

$$\langle T \rangle = N^{-1} \int_0^\infty dx \int_{-\infty}^\infty dx' (x' - u)^2 f(x, x', z) \tag{59}$$

is proportional to the mean quasi-thermal energy. For a cold beam during the period of laminar particle motion given by Eq. (17), there is no thermal term in Eq. (58); all the emittance is due to the term in brackets. We can write

$$\epsilon_{\text{total}}^2 = \epsilon_{\text{thermal}}^2 + \epsilon_{\text{fluid}}^2.$$

Now we are ready to discuss warm beams, for which the initial temperature $T_0 \equiv \langle T \rangle(0) > 0$. Davidson and Schram[8] have analyzed the closely related problem of an infinite 1-D plasma. They showed that small-amplitude fluid motion is unaffected by finite temperature, except for a frequency shift of order $\kappa^2 \lambda_D^2$, providing $\kappa^2 \lambda_D^2$ is small; κ is the wave number of a sinusoidal disturbance and λ_D is the Debye length. We adapt their results to our case by writing their small-temperature parameter as $\pi^2 T_0 / k^2 h^2$. Their results apply if our initial temperature is small, i.e., if $T_0 \ll k^2 h^2 / \pi^2$. For such a beam, Eq. (42) still applies to the fluid part of the emittance if a slight correction[8] is made to k.

Results obtained by linearization are often useful and are sometimes quite accurate, even in cases where the small parameters are not particularly small. Our warm-beam problem provides an excellent illustration of this phenomenon. Numerical simulations show that, even when the temperature parameter is fairly large, i.e., when $T_0 \cong k^2 h^2 / \pi^2$, the fluid motion is unaffected except for the above-mentioned k correction. This remains true even for large variations in the initial density profile (we restrict ourselves here to the period of initial emittance growth). The correction to k predicted by Ref. 8 is still remarkably accurate under such conditions. (Details of this result and the results of other numerical simulations, performed in collaboration with L. Soroka, will be reported separately.)

We can now quantify the term "warm beam" used throughout this section: A warm beam has a finite initial temperature T_0 which does not much exceed $k^2 h^2 / \pi^2$.

If the beam is mismatched, there will be significant variation in the envelope size, which will cause compressional heating (or cooling) and variation in $\langle x^2 \rangle \langle T \rangle$. But if the beam is matched, the term $\langle x^2 \rangle \langle T \rangle$ will be essentially constant, so that $\epsilon_{\text{th}}(z) = \epsilon_0$, where $\epsilon_0 \equiv X_0^2 T_0$ is the initial thermal emittance. Then, since Eq. (42) applies to the fluid part of the emittance, we can write

$$\epsilon_{\text{tot}}^2 = \epsilon_0^2 + \epsilon_{\text{fluid}}^2(z)$$

or

$$\epsilon_{\text{tot}}(z) = \left(\epsilon_0^2 + \frac{P}{\sqrt{3}} X_0^3 U_{n0} \sin^2 k_1 z \right)^{1/2}, \tag{60}$$

where k_1 is the channel wave number k with the correction of order $\pi^2 T_0/k^2 h^2$ mentioned above; see Ref. 8. Equation (60) is consistent with the moment-equation result of Appendix A [Eq. (A-25)] if the beam becomes uniform at $z = \lambda_1/4$; $\lambda_1 \equiv 2\pi/k_1$. This uniformity is exact for a cold beam and, according to the above discussion, is essentially exact for a warm beam.

Equation (60) resembles a sheet-beam version of an equation due to Struckmeier, Klabunde, and Reiser—see Eq. (15) in Ref. 4. What is new in Eq. (60) is that it shows that the upper limit mentioned in Ref. 4 is actually reached and shows that it is reached at $z = \lambda_1/4$.

3. ROUND BEAMS

Exact expressions for the time dependence of rms emittance, such as Eq. (42), are not obtainable for round beams. However, rather accurate results can be derived from perturbation analysis. Although the results are similar to the sheet-beam case, there are several differences, the most noteworthy of which are the following:

(i) The critical density for laminar particle motion is again half the equivalent uniform density, with a first-order correction, typically around 10%.
(ii) Different parts of a nonuniform round beam oscillate at slightly different frequencies. The correction is of second order (usually less than 1%), with negligible effect, except perhaps for long time scales. The fundamental frequency for a cold beam is essentially ω_0 where $\omega_0^2 = 2k^2$.
(iii) The particle oscillations are nonlinear, so the beam density is not precisely uniform at $z = \lambda_0/4$, where $\lambda_0 = 2\pi/\omega_0$. However, the nonuniformity is so small that essentially all the free self-field energy is converted into kinetic energy and emittance growth.

Again, we start with cold beams and discuss thermal effects later.

3.1. Round-Beam Particle Dynamics

If the beam density is $n(r, z)$, the number of particles per centimeter of length within radius r is

$$N_r(r, z) = \int_0^r 2\pi r\, n(r_1, z)\, dr_1, \tag{61}$$

and the total number per centimeter of length is

$$N = \int_0^\infty 2\pi r\, n(r, z)\, dr. \tag{62}$$

The self-field

$$E_s = 2eN_r/r \tag{63}$$

is proportional to the total perveance K, given by

$$K = 2Ne^2/mv^2. \tag{64}$$

As with sheet beams, the external focusing force F_e is assumed to be linear. We define k^2 by

$$F_e/mv^2 = -k^2 r \tag{65}$$

and get

$$r'' + k^2\left(r - \frac{K}{k^2}\frac{N_r(r, z)}{Nr}\right) = 0. \tag{66}$$

For a cold beam, the particle motion is laminar for z less than a critical distance z_C. We write ρ for the initial position of the particle that is currently at $r(z)$; thus, $N_r(r, z) = N_r(\rho, 0)$. Using the abbreviation $N_r(\rho, 0) = N_r(\rho)$, we define the equilibrium position r_e, which is constant for each particle in laminar motion:

$$r_e(\rho) = \left(\frac{K}{k^2}\frac{N_r(\rho)}{N}\right)^{1/2}. \tag{67}$$

Then

$$r'' + k^2\left(r - \frac{r_e^2}{r}\right) = 0 \tag{68}$$

in the laminar range. A cold beam may have a well-defined edge initially, where the density falls to zero. If we call this edge-radius a, then

$$r_e(a) = (K/k^2)^{1/2}. \tag{69}$$

Next, in order to expand Eq. (68), we define

$$\omega_0^2 = 2k^2 \tag{70}$$

and

$$y(\rho) = (r - r_e)/r_e, \tag{71}$$

the normalized deviation from equilibrium. The initial value of y is

$$\eta(\rho) \equiv \rho/r_e(\rho) - 1. \tag{72}$$

According to Eqs. (61) and (67), this important parameter vanishes for all ρ if the beam is matched and uniform. It turns out to be small everywhere for most nonuniform profiles if the beam mismatch is not too large.

Substituting Eqs. (70) and (71) into (68) and expanding,

$$y'' + \omega_0^2\left(y - \frac{y^2}{2} + \frac{y^3}{2} - \cdots\right) = 0. \tag{73}$$

This can be solved by the Lindstedt–Poincaré method discussed in Ref. 9. We use slightly different notation here, calling the expansion parameter δ. The solution,

for the initial condition $r'(\rho) = 0$, is

$$r(\rho, z) = r_e\left(1 + \delta \cos \omega z + \frac{\delta^2}{4}(1 - \tfrac{1}{3}\cos 2\omega z) + \cdots\right), \tag{74}$$

where

$$\delta(\rho) = \eta - \eta^2/6, \tag{75}$$

$$\omega(\rho)/\omega_0 = 1 + \delta^2/12. \tag{76}$$

The next term in Eq. (74) is of order δ^3. We shall calculate various beam quantities to first order in η; therefore, ω is replaced by ω_0 in the following discussion.

We evaluate $dr/d\rho$ in the next section. To obtain first-order accuracy, we need to keep the second-order terms in Eqs. (74) and (75). Defining $\lambda_0 = 2\pi/\omega_0$, we have

$$r(a, \lambda_0/4) = r_e(a)(1 + \delta^2/3), \tag{77}$$

so that to first order, $(K/k^2)^{1/2}$ is the beam radius at $z = \lambda_0/4$.

Differentiating Eq. (74) with respect to z, we find to first order

$$r'(\rho, z) = -\omega_0(\rho - r_e) \sin \omega_0 z\left(1 - \frac{\eta}{6} - \frac{\eta}{3}\cos \omega_0 z\right), \tag{78}$$

which we shall use later.

3.2. *Crossing of Trajectories in Round Beams*

Laminar particle motion ceases at the critical distance z_C, where the derivative $dr(\rho, z_C)/d\rho$ first vanishes. We find, after some algebra,

$$\frac{dr}{d\rho} = \frac{dr_e}{d\rho} + \left(1 - \frac{dr_e}{d\rho}\right)\left[C + \frac{\eta}{3}(2 - C - C^2)\right], \tag{79}$$

where $C = \cos \omega_0 z$. From Eqs. (61) and (67),

$$\frac{r_e}{\rho}\frac{dr_e}{d\rho} = \frac{n(\rho)}{n_u}, \tag{80}$$

where for a round beam

$$n_u = \frac{N}{\pi K/k^2}. \tag{81}$$

Using Eqs. (74), (79), and (80),

$$\frac{r\,dr}{\rho\,d\rho} = \frac{n(\rho)}{n_u} + \left(1 - \frac{n(\rho)}{n_u}\right)(C + \tfrac{2}{3}\eta(1 - C)^2). \tag{82}$$

The condition for trajectory crossing is found by setting the left side equal to zero

and solving for $\cos \omega_0 z_C$. The result is the same as for sheet beams except for a correction factor, which we give to first order.

Laminarity criterion. If $n(\rho) > n_u/2(1 - \frac{4}{3}\eta)$ for all $\rho < a$, z_C does not exist, and the motion is laminar for all z in the cold-beam limit.

As with sheet beams, if z_C exists, then it is less than $\lambda_0/2$. However, as the minimum $n(\rho)$ decreases to zero, z_C does not approach $\lambda_0/4$ but rather $(1 + 4\eta_C/3\pi)(\lambda_0/4)$; η_C is calculated at the location ρ_C with the lowest initial density.

Of course, Eq. (68) is invalid if and when crossing occurs. In the case of smooth density profiles, this occurs after $\lambda_0/4$, but analysis shows that there are discontinuous profiles where wave breaking precedes $\lambda_0/4$.

3.3. Beam Density Time Dependence

By analogy with the sheet-beam case, laminarity can be expressed as

$$2\pi r\, n(r, z)\, dr = 2\pi\rho\, n(\rho)\, d\rho \tag{83}$$

or

$$\frac{r}{\rho}\frac{dr}{d\rho} = \frac{n(\rho)}{n(r, z)}, \tag{84}$$

and Eq. (82) gives

$$n(r, z) = \frac{n(\rho)}{\dfrac{n(\rho)}{n_u} + \left[1 - \dfrac{n(\rho)}{n_u}\right][C + \frac{2}{3}\eta(1 - C)^2]}, \tag{85}$$

where the r dependence is obtained by simultaneous use of Eq. (74). See the discussion under Eq. (19). If the laminarity criterion is violated, shocklike behavior (see Fig. 1) will begin at $z = z_C$ if the initial profile is continuous.

3.4. Rms Beam Size and Matching

Because of the nonlinearity of Eq. (73), the solution, Eq. (74), shows a complicated time behavior. We shall not consider the exact time dependence of $\langle r^2 \rangle$, but simply calculate this and other averages at $z = \lambda_0/4$. We show later that at this point the density profile is nearly uniform, so that essentially all of the free self-field energy is converted into emittance growth.

For a round beam, averages over density profiles are defined by

$$\langle g \rangle(z) = N^{-1} \int_0^\infty dr\, 2\pi r\, n(r, z) g(r). \tag{86}$$

Using Eq. (83), we change the integration variable from the current position r to

the initial value ρ and find

$$\langle g\rangle(z) = N^{-1}\int_0^a d\rho 2\pi\rho n(\rho) g(r(\rho, z)). \tag{87}$$

The initial mean square radius, at $z = 0$, is

$$R_0^2 = \langle\rho^2\rangle = N^{-1}\int_0^a d\rho 2\pi\rho^3 n(\rho). \tag{88}$$

At $z = \lambda_0/4$, Eq. (74) gives, after we drop the second-order term in η,

$$\langle r^2\rangle(\lambda_0/4) = \langle r_e^2\rangle, \tag{89}$$

where the notation on the left means that the average of r^2 is evaluated at $z = \lambda_0/4$. Equations (80) and (87) give

$$\langle g\rangle(z) = N^{-1}2\pi n_u\int_0^a d\rho r_e\frac{dr_e}{d\rho} g(r(\rho, z)), \tag{90}$$

so that

$$\langle r_e^2\rangle = \frac{K}{2k^2}, \tag{91}$$

and the condition for $\lambda_0/4$ matching, using Eq. (89), is

$$R_0^2 = \frac{K}{2k^2}. \tag{92}$$

3.5. Peak Rms Emittance

At least three different definitions of rms emittance for two-dimensional beams have appeared in the literature, in papers by Sacherer,[2] by Lapostolle,[1] and by Lee *et al.*[3] Sacherer's definition is

$$\epsilon = (\langle x^2\rangle\langle x'^2\rangle - \langle xx'\rangle^2)^{1/2}.$$

If the beam is not round, then this is called ϵ_x and there is a similar expression for ϵ_y. Lapostolle's definition is the same except that it is four times larger in order to agree with the enclosure emittance for the K–V distribution. (To avoid confusion, it is wise to use a special notation. For example, Ref. 10 uses the informative symbol $\epsilon_{4\text{rms}}$.) Lee's definition, applicable only to round beams, is

$$\epsilon_{\text{Lee}} = (\langle r^2\rangle\langle r'^2\rangle - \langle rr'\rangle^2)^{1/2},$$

which is twice Sacherer's since $\langle x^2\rangle = \langle y^2\rangle = \langle r^2\rangle/2$. For present purposes Lee's definition would be convenient, but since we have already used Sacherer's for sheet beams, we shall also use it for round beams. In terms of the radial coordinate, Sacherer's emittance is

$$\epsilon = \tfrac{1}{2}(\langle r^2\rangle\langle r'^2\rangle - \langle rr'\rangle^2)^{1/2}. \tag{93}$$

From Eq. (78),

$$r'(\lambda_0/4) = -\omega_0(\rho - r_e)(1 - \eta/6),$$

but, since $\rho - r_e = r_e\eta$, we have, to first order in η,

$$r'(\lambda_0/4) = -\omega_0 r_e\eta = -\omega_0(\rho - r_e). \tag{94}$$

Recalling that to first order $r(\lambda_0/4) = r_e$, we readily find

$$\epsilon^2(\lambda_0/4) = (\omega_0^2/4)(\langle r_e^2\rangle\langle\rho^2\rangle - \langle r_e\rho\rangle^2). \tag{95}$$

(We have not assumed that the beam is matched.) Two of the averages on the right have been calculated already. It remains to find the quantity $\langle r_e\rho\rangle$. Using Eq. (90) and integrating by parts,

$$\langle r_e\rho\rangle = \left(\frac{2K}{3k^2}\right)^{1/2}\left\{a - \int_0^a d\rho\left[\frac{N_r(\rho)}{N}\right]^{3/2}\right\}. \tag{96}$$

Given an initial density profile $n(\rho)$, we can calculate $\epsilon(\lambda_0/4)$ to first order in η by using Eqs. (95), (88), (91), and (96). We offer an example in Section 3.7. But first we show a different way to calculate $\epsilon(\lambda_0/4)$ for the special case of a matched beam.

3.6. Peak Emittance from Free Self-Field Energy

Recall that the exact solution for sheet beams, Eq. (42), turned out to be closely related to the differential equation for emittance, Eq. (A-25). In the case of round beams, this differential equation is[1,3,4]

$$\frac{d}{dz}\epsilon^2 = -\frac{K}{16}R^2\frac{d}{dz}U_n, \tag{97}$$

where

$$R^2(z) = \langle r^2\rangle = 2\langle x^2\rangle$$

and where the normalized free energy U_n (round beams) is

$$U_n(z) = 4\int_0^b drN_r^2(z)/N^2r - (1 + 4\ln b/R\sqrt{2}). \tag{98}$$

The upper limit b is chosen large enough to include all of the beam. In Ref. 4, Eq. (97) was integrated by treating R as constant. This yielded a maximum emittance growth:

$$\Delta\epsilon^2(\max) = \frac{K}{16}R_0^2U_{n0}, \tag{99}$$

where

$$U_{n0} = 4\int_0^a d\rho N_r^2(\rho)/N^2\rho - (1 + 4\ln a/R_0\sqrt{2}). \tag{100}$$

(Note that the upper limit is the actual initial beam radius a.) The method of analysis used in Refs. 1, 3, and 4 did not show how rapidly the maximum emittance would be reached. But we recall that for sheet beams all of the free self-field energy is converted into emittance growth at one quarter of a plasma period. This is very nearly true for round beams as well. It can be shown that to a good approximation for a matched beam

$$\epsilon^2(\lambda_0/4) = \frac{K}{16} R_0^2 U_{n0}. \tag{101}$$

It is interesting to compare this result with Eq. (95) and its associated equations. In Eq. (98) we integrated the square of N_r, whereas Eq. (96) involves the 3/2 power. We show in the next section [Eq. (113)] that the two methods give nearly identical results. But first we show for a typical density profile that the density at $\lambda_0/4$ is nearly uniform. This indicates that in round beams essentially all of the free energy is converted at $\lambda_0/4$ into fluid energy and explains the agreement of the different methods.

3.7. Parabolic Profile

A simple model for a nonuniform beam is the initial density profile

$$\eta(\rho) = \frac{2N}{\pi a^2}\left(1 - \frac{\rho^2}{a^2}\right). \tag{102}$$

Then

$$N_r(\rho) = \frac{2\rho^2}{a^2} N\left(1 - \frac{\rho^2}{2a^2}\right). \tag{103}$$

From Eq. (88),

$$R_0^2 = a^2/3, \tag{104}$$

and the matching condition, Eq. (92), is

$$a^2 = \frac{3}{2}\frac{K}{k^2}. \tag{105}$$

Then, using Eq. (81), the beam is matched if

$$n(\rho) = \tfrac{4}{3} n_u\left(1 - \frac{\rho^2}{a^2}\right). \tag{106}$$

From Eqs. (67) and (72),

$$\eta(\rho) = -1 + \frac{\sqrt{3}}{2}\left(1 - \frac{\rho^2}{2a^2}\right)^{-1/2}. \tag{107}$$

The extreme values are

$$\eta(0) = -0.134,$$
$$\eta(a) = +0.225.$$

The neglected terms of order η^2 in Eqs. (75–77) have small coefficients, so that Eq. (107) predicts errors of 1% or less in the following calculations.

To find the density profile at $\lambda_0/4$, we set $C = 0$ in Eq. (85):

$$\eta(\rho, \lambda_0/4) = \frac{n_u}{1 + \left[-1 + \frac{n_u}{n(\rho)}\right]\frac{2}{3}\eta}. \tag{108}$$

To get $n(r)$, we need to combine this with $r(\rho, \lambda_0/4)$ from Eq. (89). Using Eqs. (67) and (103), we have

$$r^2(\lambda_0/4) = \frac{4\rho^2}{3}\left(1 - \frac{\rho^2}{2a^2}\right), \tag{109}$$

which may be solved for ρ. If we define

$$G(r) = \left(1 - \frac{3r^2}{2a^2}\right)^{1/2}, \tag{110}$$

then the solution is

$$\rho^2/a^2 = 1 - G(r). \tag{111}$$

Inserting this in Eqs. (102), (107), and (108) gives

$$n(r, \lambda_0/4) = \frac{n_u}{1 + \left(1 - \frac{3}{4G}\right)\frac{2}{3}\left[1 - \frac{\sqrt{2}}{\sqrt{3}}(1+G)^{-1/2}\right]}, \tag{112}$$

This result is plotted in Fig. 3, where it is compared with the initial profile. The density is clearly flat enough at $z = \lambda_0/4$ to make $U_n(z)$ negligible. Thus, Eq. (99) gives an accurate result. Inclusion of second-order corrections would change the shape in Fig. 3 slightly but would not change our conclusion.

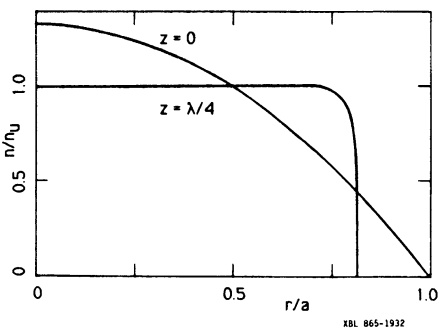

FIGURE 3 Density profiles at $z = 0$ and $z = \lambda_0/4$ for a round beam with parabolic initial density profile.

To confirm this point, we calculated the emittance at $z = \lambda_0/4$ using the free energy U_{n0}, Eq. (101), and compared it with the result obtained from the dynamics, Eqs. (95) and (96). We found

$$\epsilon(\lambda_0/4) = 0.0374\, R_0\sqrt{K} \tag{113a}$$

and

$$\epsilon(\lambda_0/4) = 0.0375\, R_0\sqrt{K}, \tag{113b}$$

respectively. The uniformity at $\lambda_0/4$ (Fig. 3) is responsible for the high accuracy of the free-energy calculation.

3.8. *Typical Numbers*

When comparing calculations with experimental data, Lapostolle's emittance definition[1] is advantageous and is often used. We follow the Los Alamos notation[10] and define

$$\epsilon_{4\text{rms}} = 4\epsilon. \tag{114}$$

We multiply $\epsilon_{4\text{rms}}$ (nonrelativistically) by β to get $\epsilon_{N4\text{rms}}$, the normalized emittance. Then Eq. (101) gives, at the point $z = \lambda_0/4$,

$$\epsilon_{N4\text{rms}} = 0.68 \times 10^6 \beta (U_{n0})^{1/2} \left(\frac{Ia^2}{V^{3/2}}\right)^{1/2}$$

π mrad-cm. The beam current I is in amperes, and V is in volts. (For Q and $A \neq 1$, see Section 2.)

Particular case. 200 mA D^- beam at 100 keV:

$$\epsilon_{N4\text{rms}} = 0.50\,(U_{n0})^{1/2} a \qquad [\pi \text{ mrad-cm}].$$

For a parabolic profile, $n \cong 1 - r^2/a^2$, we have (see Table A-I in appendix A) the shape factor $U_{n0} = 0.0224$, so that

$$\epsilon_{N4\text{rms}} = 0.074a \qquad [\pi \text{ mrad-cm}].$$

For some applications this could be excessive, and a more uniform beam would be required.

3.9. *Inclusion of Thermal Emittance*

Warm round beams can be treated in the same way as warm sheet beams by splitting the mean square emittance into a thermal part and a fluid-flow part. For a matched, strongly space-charge-dominated beam, the total emittance at $z \cong \lambda_0/4$ is

$$\epsilon_{\text{tot}} = \left(\epsilon_0^2 + \frac{K}{16} R_0^2 U_{n0}\right)^{1/2}. \tag{115}$$

See the discussion in Section 2.14.

Simulation studies by C. M. Celata[11] have confirmed that Eq. (115) gives accurate results when the two terms enclosed by parentheses are about the same size.

Our prediction that the emittance peaks at $z \cong \lambda_0/4$ agrees with the simulation results reported by Wangler *et al.*;[4] in fact, the present study was inspired by a desire to understand the physics behind those surprising results.

ACKNOWLEDGMENTS

I wish to thank Chris Celata for her interest in these ideas and for persistently urging me to write them up. I thank her, Ed Lee, and Bill Cooper for reading parts of the manuscript and for offering helpful criticism. I am also grateful to the anonymous reviewer who made a number of valuable suggestions which helped the clarity of this paper. And I thank Ludmilla Soroka for collaborating on numerical simulations that supported and extended the analytical work reported here.

This work was supported by the U.S. Department of Energy under DE-AC03-76SF00098.

REFERENCES

1. P. M. Lapostolle, *Energy Relationships in Continuous Beams,* CERN report CERN-ISR-DI/71-6 (1971). P. M. Lapostolle, *IEEE Trans. Nucl. Sci.* **18,** 1101 (1971).
2. F. J. Sacherer, *IEEE Trans. Nucl. Sci.* **18,** 1055 (1971).
3. E. P. Lee, S. S. Yu, and W. A. Barletta, *Nucl. Fusion* **21,** 961 (1981).
4. T. P. Wangler, K. R. Crandall, R. S. Mills, and M. Reiser, *IEEE Trans. Nucl. Sci.* **32,** 2196 (1985). This paper lists many other important references on emittance growth. It is partly based on J. Struckmeier, J. Klabunde, and M. Reiser, *Particle Accelerators* **15,** 47 (1984).
5. I. B. Bernstein and S. K. Trehan, *Nucl. Fusion* **1,** 3 (1960). This long review paper includes a short section on nonlinear oscillations, based mainly on the work of John Dawson, for which references are given. Dawson in his paper refers to fine-scale mixing rather than wave breaking.
6. O. A. Anderson, D. G. Kane, and L. Soroka, *Bull. Am. Phys. Soc.* **30,** 1595 (1985).
7. O. A. Anderson, *AIP Conf. Proc.* **111,** 473 (1983).
8. R. C. Davidson and P. P. Schram, *Nucl. Fusion* **8,** 183 (1968).
9. A. H. Nayfeh and D. T. Mook, *Nonlinear Oscillations* (John Wiley and Sons, New York, 1979).
10. R. Keller, J. D. Sherman, and P. Allison, *IEEE Trans. Nucl. Sci.* **32,** 2579 (1985).
11. C. M. Celata, personal communication, Lawrence Berkeley Laboratory, December 1985.

APPENDIX A

Moment Equations for Sheet Beams

Lapostolle,[1] Lee,[3] and Wangler *et al.*[4] used moment equations for round beams to obtain a differential equation relating changes in emittance to changes in self-field energy. In this appendix, we use the same technique for sheet beams and compare the results.

Just as in Section 2, we make several assumptions to simplify the notation; see the Introduction. And again, we assume the external focusing force F_e to be linear. But we do not need to assume that it is constant; to emphasize this point, we change notation and replace the constant k^2 by the symbol K_e, where K_e may depend on z.

Another advantage of the moment-equation approach is that it applies to beams of arbitrary temperature. As discussed at the end of this appendix, the cost of these generalizations is the loss of information on the *rate* at which the emittance changes.

A-1. PARTICLE MOTION

The transverse force can be written as $F_x = eE_s + F_e$, where $F_e(z)$ is the linear external force. Then

$$x'' \equiv d^2x/dz^2 = eE_s/mv^2 + F_e/mv^2. \tag{A-1}$$

Defining K_e and K_s by

$$F_e/mv^2 = -K_e(z)x, \tag{A-2}$$

$$eE_s/mv^2 = K_s(x, z)x, \tag{A-3}$$

we can write

$$x'' = [K_s(x, z) - K_e(z)]x, \tag{A-4}$$

which can be put into two other useful forms:

$$(x^2)''/2 = x'^2 + (K_s - K_e)x^2, \tag{A-5}$$

$$(x'^2)' = (K_s - K_e)(x^2)'. \tag{A-6}$$

In terms of quantities defined at the beginning of Section 2,

$$K_s x = PN_x/N. \tag{A-7}$$

A-2. ENVELOPE EQUATION

We define averages here in the same way they are defined in Ref. 3. If some quantity associated with the ith particle in a moving beam slice containing N particles is $g_i = g(x_i, x_i', z)$, then

$$\langle g \rangle = (1/N) \sum_N g_i. \tag{A-8}$$

Define

$$X^2 = \langle x^2 \rangle, \tag{A-9}$$

$$V^2 = \langle x'^2 \rangle. \tag{A-10}$$

Note that $X^{2\prime} = N^{-1} \sum_N (x_i^2)' = N^{-1} \sum_N 2x_i x_i'$, so that

$$XX' = \langle xx' \rangle. \tag{A-11}$$

Equations (A-5), (A-6), (A-9), and (A-10) now give

$$(X^2)''/2 = V^2 + \langle K_s x^2 \rangle - K_e X^2, \tag{A-12}$$

$$(V^2)' = \langle K_s x^{2\prime} \rangle - K_e X^{2\prime}. \tag{A-13}$$

The rms emittance is defined by Eq. (39). Using Eqs. (A-9)–(A-11), we get the alternative expression

$$\epsilon^2 = X^2(V^2 - X'^2). \tag{A-14}$$

Equations (A-12) and (A-14) give the rms envelope equation

$$X'' + K_e(z)X = \epsilon^2/X^3 + W(z)/X, \tag{A-15}$$

where $W(z)$ is the virial moment[3] (not a constant here as it is in the 2-D case):

$$W(z) = \langle K_s x^2 \rangle. \tag{A-16}$$

To calculate averages of this type, we use

$$\langle g \rangle(Z) = N^{-1} \int_0^\infty dx\, n(x, z) g(x), \tag{A-17}$$

which is equivalent to Eq. (A-8). Then Eqs. (A-16) and (A-7) give

$$W(z) = \langle N_x x \rangle P/N = (P/N^2) \int_0^\infty dx (\partial N_x/\partial x) N_x x.$$

Integrating by parts, we find

$$W(z) = (P/2N^2) \int_0^b dx (N^2 - N_x^2). \tag{A-18}$$

Since $N^2 - N_x^2 \to 0$ for x outside the beam, we have replaced the upper limit by a finite distance b for later convenience.

A-3. EMITTANCE GROWTH

According to Eqs. (A-13) through (A-15),

$$\epsilon^{2\prime} = X^2 \langle K_s x^{2\prime} \rangle - X^{2\prime} W(z), \tag{A-19}$$

which is most easily derived by differentiating ϵ^2/X^2. To evaluate the average in the above equation, we follow Ref. 3 and note that $\langle K_s x^{2\prime} \rangle = 2\langle K_s x u \rangle$, where u is the local average of x'. The beam fluid velocity in the x direction is vu [Eq. (56)]. Steady flow implies $\mathbf{v} \cdot \nabla N_x = 0$, or

$$\partial N_x/\partial z = -nu$$

at any value of x. Then, using Eqs. (A-7) and (A-17),

$$\begin{aligned}\langle K_s x^{2\prime}\rangle &= (2P/N)\langle N_x u\rangle \\ &= (2P/N^2)\int_0^\infty dx\, nuN_x \\ &= -(2P/N^2)\int_0^\infty dx N_x \partial N_x/\partial z \\ &= -(P/N^2)(d/dz)\int_0^b dx N_x^2,\end{aligned}$$

where again a finite distance $b \gg X$ is used for the upper limit without affecting the result. Comparing this with Eq. (A-18) shows that

$$\langle K_s x^{2\prime}\rangle = 2W', \tag{A-20}$$

so

$$\epsilon^{2\prime} = 2X^2 W' - 2XX'W$$

or

$$\epsilon^{2\prime} = X^3(2W/X)'. \tag{A-21}$$

A-4. SELF-FIELD ENERGY

Equation (A-18) can be written, using Eq. (3), as

$$W(z) = Pb/2 - (P/2)\int_0^b dx E_s^2/E_0^2,$$

where

$$E_0 = 4\pi eN$$

is essentially the self-field outside the beam. Rearrangement gives the self-field energy

$$\int_0^b dx E_s^2/8\pi = (b - 2W/P)E_0^2/8\pi. \tag{A-22}$$

We show in Appendix B that, for a given rms beam size X, the field energy is minimized as the beam profile approaches uniformity. Therefore, the available field energy is obtained by subtracting from Eq. (A-22) the energy for a uniform distribution having the same P and the same local x. The (half) width of the uniform distribution is

$$X\sqrt{3}, \tag{A-23}$$

while its self-field energy is

$$(b - 2X/\sqrt{3})E_0^2/8\pi.$$

Subtracting from Eq. (A-22) gives the available, or free, self-field energy

$$2(X/\sqrt{3} - W/P)E_0^2/8\pi.$$

A dimensionless parameter $U_n(z)$, proportional to the free self-field energy, is obtained by dividing the above expression by the self-field energy contained within the comparable uniform distribution. The result is

$$U_n(z) = 2(1 - \sqrt{3}W/PX), \tag{A-24}$$

the normalized free energy. It is seen from Eq. (A-18) that $U_n(z)$ depends only on the beam profile, so it may also be referred to as the beam shape factor.

The emittance growth, then, using Eq. (A-21), is

$$\frac{d}{dz}\epsilon^2 = -\frac{P}{\sqrt{3}}X^3\frac{d}{dz}U_n. \tag{A-25}$$

This is similar to the result for round beams[3,4]

$$\frac{d}{dz}\epsilon^2 = -\frac{K}{16}R^2\frac{d}{dz}U_n. \tag{A-26}$$

The rms radius R, perveance K, and shape factor U_n are defined in the main text. The last of these can be written in a way that emphasizes its relationship to self-field energy:

$$U_n = \int_0^b dr\, rE_s^2/N^2e^2 - (1 + 4\ln b/R\sqrt{2}). \tag{A-27}$$

Table A-I compares the sheet-beam and round-beam shape factors for uniform, parabolic, tent-shaped, hollow parabolic, and delta-function profiles. Appendix B shows that the uniform profile gives the smallest possible U_n, namely, zero.

Column 1 of Table A-I gives the (unnormalized) density profile $n(y)$, where $y = x/h$ for a sheet beam and $y = r/a$ for a round beam; h and a are the outer dimensions. It is understood that $n(y) = 0$ for $y > 1$.

Unlike Eqs. (42) and (101), Eqs. (A-25) and (A-26) give no information on

TABLE A-I

Sheet-beam and round-beam shape factors for different profiles

	Sheet beam		Round beam		
Profile, $n(y)$	X^2	U_n^{sheet}	R^2	U_n^{round}	Ratio, U^r/U^s
1	$h^2/3$	0	$a^2/2$	0	
$1-y^2$	$h^2/5$	0.0082	$a^2/3$	0.0224	2.74
$1-y$	$h^2/6$	0.0201	$3a^2/10$	0.0450	2.24
y^2	$3h^2/5$	0.0834	$2a^2/3$	0.0754	0.90
$\delta(1-y)$	h^2	0.2679	a^2	0.3863	1.44

time dependence, since the moment equations on which they are based are not closed. They do have the feature of being valid for cases with variable focusing force. However, although they are perfectly general (for the model stated in the Introduction), they are mainly useful in cases exhibiting fluctuations sufficiently small that X (or R) can be treated as constant. One way to obtain small fluctuations is to adjust the perveance of the nonuniform beam so that it equals the perveance of a uniform matched beam having the same X or R. As discussed in Ref. 7, for example, such matching is based on $K_e(z)$ averaged over a structure period.

APPENDIX B

Minimum Self-Field Energy

Proposition: the normalized self-field energy

$$I = \int_0^b dx E_s^2/E_0^2 = \int_0^b dx N_x^2/N^2 \tag{B-1}$$

of any nonuniform beam with profile $n(x)$ is greater than I_u, where I_u is calculated for a uniform profile having the same X.

As before, b is chosen large enough that $n = 0$ for $x \geq b$.

Definition:

$$f(x) = n(x) - n_u(x), \tag{B-2}$$

where

$$n_u(x) = (N/a)[1 - H(x - a)], \tag{B-3}$$

and H is the Heaviside step function. We note that

$$a = X\sqrt{3}. \tag{B-4}$$

Definition:

$$g(x) = \int_0^x d\xi f(\xi)/N. \tag{B-5}$$

Properties of g:

$$g(0) = g(b) = 0, \tag{B-6}$$

$$g \leq 0 \quad \text{for} \quad x > a, \tag{B-7}$$

$$\int_0^b dx\, xg(x) = 0. \tag{B-8}$$

Equations (B-6) and (B-7) are obvious from the definitions. Equation (B-8) follows from the requirement that the profiles $n(x)$ and $n_u(x)$ have the same X; thus, $\int dx\, x^2 f(x) = 0$. Putting $f = dg/dx$ and integrating by parts gives Eq. (B-8).

Calculating the Self-Field Energy [*Eq.* (*B*-1)]: Since $n(x) = n_u(x) + f(x)$, we integrate to get

$$N_x/N = [x - (x-a)H(x-a)]/a + g(x). \tag{B-9}$$

We find

$$I = a^{-2}\int_0^a (x^2 + 2axg)\,dx + \int_a^b (1+2g)\,dx + \int_0^b g^2\,dx.$$

We subtract I_u as defined above (which is I with $g \to 0$):

$$I - I_u = a^{-1}\int_0^a 2xg\,dx + \int_a^b 2g\,dx + \int_0^b g^2\,dx.$$

Since the first term on the right can be written, using Eq. (B-8),

$$-a^{-1}\int_a^b 2xg\,dx,$$

we have

$$I - I_u = \int_a^b 2g(1 - x/a)\,dx + \int_0^b g^2\,dx. \tag{B-10}$$

In the first term on the right, $(1 - x/a)$ is obviously negative in the range of integration; g is negative by Eq. (B-7). Thus, the first integral is nonnegative. The second integral is positive for any nonuniform $n(x)$, and this proves the proposition.